Journal of Magnetism and Magnetic Materials 321 (2009) 247–251

Contents lists available at ScienceDirect

Journal of Magnetism and Magnetic Materials

journal homepage: www.elsevier.com/locate/jmmm

Electromagnetic properties of samarium-substituted NiCuZn ferrite prepared by auto-combustion method

P.K. Roy, J. Bera *

Department of Ceramic Engineering, National Institute of Technology, Rourkela 769 008, India

ARTICLE INFO

Article history:
Received 7 July 2008
Available online 14 August 2008

PACS:
75.50.G

Keywords:
Ceramic
Soft ferrite
Sm substitution
NiCuZn ferrite
Electromagnetic property

ABSTRACT

$Ni_{0.25}Cu_{0.2}Zn_{0.55}Sm_xFe_{2-x}O_4$ ferrite with $x = 0.00$, 0.025, 0.05 and 0.075 compositions were synthesized through the nitrate–citrate auto-combustion method. These powders were calcined, compacted and sintered at 900 °C for 4 h. Effect of Sm substitution on phase composition, microstructure and relative density were studied. Permeability, magnetic loss and AC resistivity were measured in the frequency range of 1 kHz–10 MHz. Permeability and AC resistivity were found to increase and loss decreased with Sm substitution up to $x = 0.05$. Saturation magnetization also increased up to that substitution limit. Observed variations in electromagnetic properties have been explained.

1. Introduction

NiCuZn ferrite is one of the most important magnetic materials for multilayer chip inductor (MLCI) applications due to their high electrical resistivity, low sintering temperature and high permeability [1–5]. MLCIs are applied in large amounts in various electronic circuits and they have greatly benefited the miniaturization of many latest electronic products, including mobile phones, notebook computers and video cameras. The chip inductor is fabricated by putting alternate layers of ferrite and silver electrode. This multilayer ceramic–metal composite should be co-fired below 950 °C to suppress the interfacial diffusion of Ag–metal into ceramics as the melting point of Ag is 961 °C. NiCuZn ferrite is used in this application because it can be sintered below 950 °C.

Better magnetic properties of ferrite are essential for modern MLCIs to reduce the number of ferrite layer in the chip and thus more miniaturization of the component is feasible. The magnetic properties of these ferrites are determined not only by their chemical composition but also by the presence of small additive and microstructure [6–9] i.e., grain size, porosity and specially grain boundary characteristics like elastic strain field due to interstitial Cu precipitation, etc. Small amount of additives are often used to modify microstructure and hence magnetic properties. Rare earth oxides are becoming promising additives to improve the magnetic properties of ferrites [10–14]. Among them, Sm-substituted CuZn ferrite [12] and La-substituted NiCuZn ferrite [14] gave promising result from the technological point of view, with a significant increase in relative permeability compared with un-substituted ferrites. Based on these results, the present work describes the effect of Sm substitution on microstructure, densification and electromagnetic properties of NiCuZn nanocrystalline ferrite prepared by combustion reaction.

2. Experimental

The ferrite powder was synthesized through nitrate–citrate auto-combustion route [15]. Analytical grade nickel nitrate [$Ni(NO_3)_2 \cdot 6H_2O$], zinc nitrate [$Zn(NO_3)_2 \cdot 6H_2O$], copper nitrate [$Cu(NO_3)_2 \cdot 3H_2O$], iron nitrate [$Fe(NO_3)_3 \cdot 9H_2O$], citric acid [$C_6H_8O_7 \cdot H_2O$] and samarium oxide [Sm_2O_3] were used to prepare $Ni_{0.25}Cu_{0.2}Zn_{0.55}Sm_xFe_{2-x}O_4$ ferrite with $x = 0.00$, 0.025, 0.05 and 0.075 compositions. Metal nitrates and citric acid solutions were prepared using deionized water. Metal nitrate solutions were standardized with respect to metal ion content through chemical analysis using ethylenediamine tetra-acetic acid (EDTA) complexometric titration. Nitrate and citric acid solutions were mixed in 1:1 M ratio of nitrate to citric acid. The pH of the solution was adjusted to 7 using ammonia solution. Then the solution was heated at 80 °C to transform into gel. When ignited at any point of the gel, the dried gel burnt in a self-propagating combustion manner until all gels were completely burnt out to form a fluffy

* Corresponding author. Tel.: +91 9437246159; fax: +91 661 2472926.
E-mail address: jbera@nitrkl.ac.in (J. Bera).

0304-8853/$ - see front matter © 2008 Elsevier B.V. All rights reserved.
doi:10.1016/j.jmmm.2008.08.051

loose ash. The auto-ignition of gel was carried out in BOROSIL glass beaker upon a hot plate.

The ash was lightly ground and calcined at 700 °C for 2 h. The calcined ferrite powder was granulated using polyvinyl alcohol as a binder and was uniaxially pressed at a pressure of 275 MPa to form toroidal and pallet specimens. The specimens were sintered at 900 °C for 4 h in air atmosphere. The bulk density and apparent porosity of sintered ferrite was measured by Archimedes principle. The as-burnt ash powders, calcined powders and the sintered ferrites were characterized with respect to phase identification, crystallite size and lattice parameter determination using X-ray diffraction (XRD) performed on Philips PW-1830 system with Cu-Kα radiation. The crystallite size was calculated from peak broadening using Scherrer formula. Microstructure of the sintered specimens was analyzed by scanning electron microscopy (SEM) and energy-dispersive X-ray spectroscopy (EDS) performed on JEOL JSM 6480 LV system. The impedance analyzer (Hewlett Packard, Model 4192A) was used to measure the inductance and the magnetic loss factor on toroids, wound with six turns enameled copper wire. The resistivity was measured on pallet samples by applying silver electrodes on the surfaces. Saturation magnetizations were measured at room temperature using Lakeshore-7040 vibrating sample magnetometer (VSM) with a maximum magnetic field of 20 kOe.

3. Results and discussion

To identify the possible formation of second phase in the NiCuZn ferrite upon Sm substitution, an XRD analysis was done. Fig. 1 shows the XRD patterns of sintered ferrites specimen with varying Sm substitutions. The most intense peaks in all the specimens were found to mach well with cubic spinel ferrite (JCPDS card no. 08-0234). Samarium iron oxide, $SmFeO_3$ phase was detected in all Sm-substituted ferrite. The amount of $SmFeO_3$, that is its' peak intensity increased with increasing Sm concentration. This apparently indicates that Sm did not form a solid solution with spinel ferrite or it has very small solid solubility. A small amount of unknown phase was found in un-substituted ferrite. The peak was tried to match with Cu and/or Cu–oxygen containing compounds. The matching suggested that the peak may be corresponding to some compound in between Cu_2O–Cu_4O_3. Many investigators reported that NiCuZn ferrite dissociates during sintering to precipitate Cu metal or its oxide [9,16]. The presence of Cu–oxygen containing phase may be due to surface oxidation of that precipitated Cu metal during sintering in air. It is interesting to note that the Cu containing compound was absent in all Sm-substituted specimen. This may be due to the solubility of precipitated Cu in $SmFeO_3$.

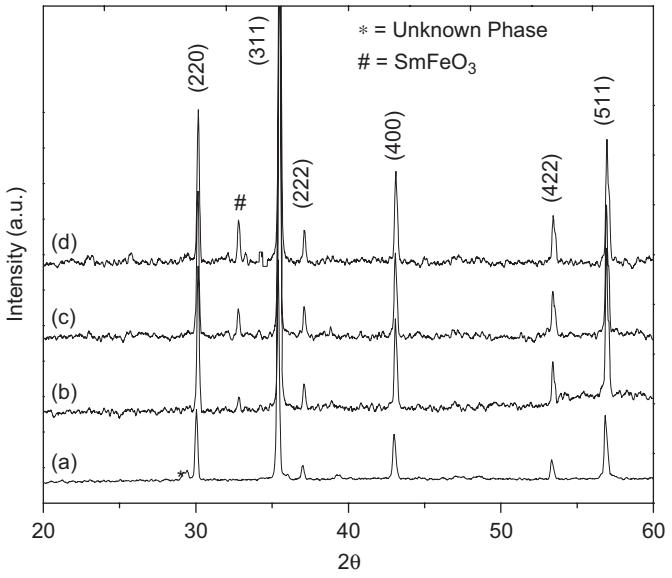

Fig. 1. XRD patterns of sintered $Ni_{0.25}Cu_{0.2}Zn_{0.55}Sm_xFe_{2-x}O_4$ ferrites with different Sm-content: (a) $x = 0.00$, (b) $x = 0.025$, (c) $x = 0.05$ and (d) $x = 0.075$.

Lattice parameters and crystallite sizes of sintered ferrite specimens, evaluated by XRD analysis, are shown in Table 1 along with their bulk density, percent theoretical density and grain size. There was a minor decrease in lattice parameter, α_0 of NiCuZn ferrite with Sm substitution, which may be due to the compressive pressure exerted on the ferrite lattice by $SmFeO_3$. Crystallite size increased with Sm substitution due to improved densification and grain growth. The density of sintered specimen increased upon Sm substitution, indicating an improved densification with the substitution. A similar trend was reported by Costa et al. [17] for Sm-substituted NiZn ferrite. Increased densification may be due to the evolution of excess Cu, Ni and Zn in the composition as Sm is substituted for Fe. Sm further takes some Fe to form $SmFeO_3$. So the neat result of Sm substitution was to create non-stoichiometry in compositions. It is known that, non-stoichiometric excess Ni, Cu and Zn are often used for low-temperature liquid-phase sintering of the ferrite [9]. For this reason the densification increased with Sm substitution.

Fig. 2 shows the microstructure of sintered specimen. Un-substituted specimen (Fig. 2A) shows the presence of a mono-phasic homogeneous microstructure with an average grain size 0.42 μm. Whereas, Sm-doped specimens (Fig. 2B–D) show a bi-phasic microstructure constituted of dark ferrite matrix grains and small whitish grain at the grain junction/boundary. EDS spectra obtained from the center of whitish grain confirmed the presence of Sm, Fe, oxygen and minor amount of Cu, Ni and Zn. This indicated whitish grains were $SmFeO_3$. The amount of $SmFeO_3$ was maximum in $x = 0.075$ composition. Average grain sizes of matrix ferrite phase are shown in Table 1. The grain size of matrix phase was maximum in $x = 0.05$ composition. Relatively lower grain size of ferrite matrix in $x = 0.075$ composition (Fig. 3D) may be due to the grain growth inhibition caused by $SmFeO_3$ [17].

Fig. 3 shows the initial permeability as a function of Sm (x) substitution in $Ni_{0.25}Cu_{0.2}Zn_{0.55}Sm_xFe_{2-x}O_4$ ferrites (the values are shown in Table 2). The permeability increased with increasing Sm (x) substitution with a maximum at $x = 0.05$ and then decreased at $x = 0.075$ composition. It is well established that permeability of polycrystalline ferrite increases with increasing density and

Table 1
Bulk density, percent theoretical density, crystallite size, lattice parameter and grain size of sintered $Ni_{0.25}Cu_{0.2}Zn_{0.55}Sm_xFe_{2-x}O_4$ ferrites with different Sm (x) content

Composition	Bulk density (gm/cm^3)	% Theoretical density	Crystallite size (nm)	Lattice parameter (Å)	Grain size (μm)
$x = 0.00$	3.75	70.74	102	8.429	0.42
$x = 0.025$	5.06	91.02	170	8.403	1.18
$x = 0.05$	5.15	93.65	184	8.392	1.21
$x = 0.075$	5.01	90.65	156	8.384	0.95

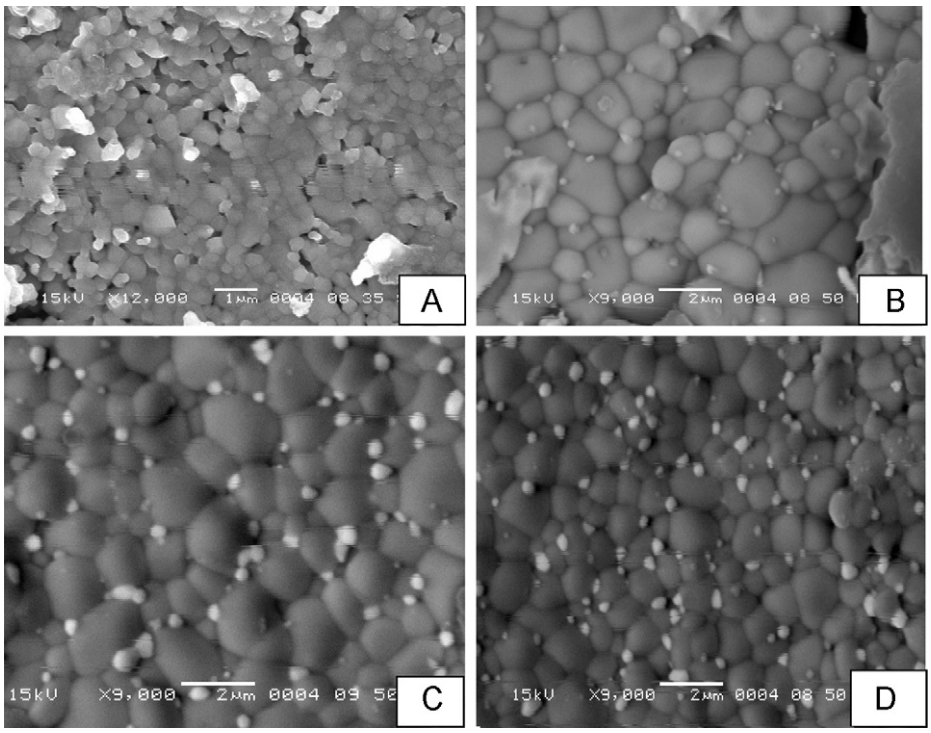

Fig. 2. SEM images of sintered $Ni_{0.25}Cu_{0.2}Zn_{0.55}Sm_xFe_{2-x}O_4$ ferrites with different Sm-content: (A) $x = 0.00$, (B) $x = 0.025$, (C) $x = 0.05$ and (D) $x = 0.075$.

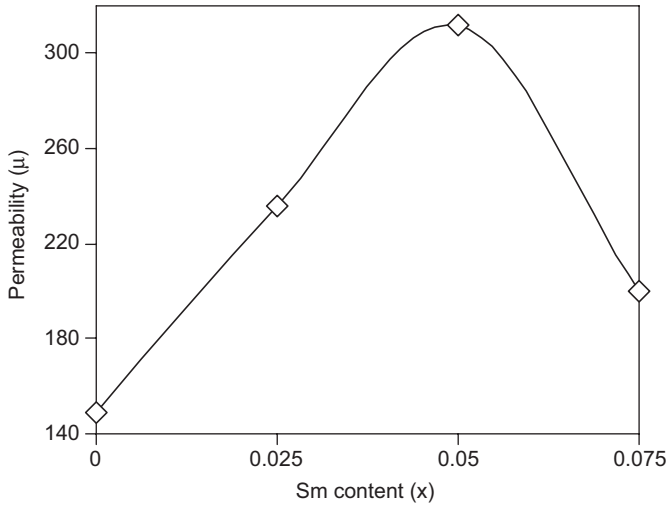

Fig. 3. Permeability as a function of Sm (x) substitution in $Ni_{0.25}Cu_{0.2}Zn_{0.55}Sm_xFe_{2-x}O_4$ ferrites.

grain size. Increase in permeability with Sm substitution may primarily be attributed to the increase in bulk density. An increase in the density, not only results in the reduction of demagnetizing field due to the reduction of pores but also raises the spin rotational contribution, which in turn increase the permeability [18]. However, the lowering of permeability in $x = 0.075$ specimen may be due to the formation of significant amount of non-magnetic $SmFeO_3$ phase and decreased grain size (Table 1) in the ceramics.

Fig. 4 shows the frequency dependence permeability of $Ni_{0.25}Cu_{0.2}Zn_{0.55}Sm_xFe_{2-x}O_4$ ferrites. Permeabilities were stable in the frequency range 100 kHz to about 2 MHz and dispersion occurred after that. That dispersion shifted to higher frequency with decreasing permeability of the specimen. The dispersion behavior can be explained by Snoek's law that cut-off frequency is

Table 2
Permeability, saturation magnetization and AC resistivity of sintered $Ni_{0.25}Cu_{0.2}Zn_{0.55}Sm_xFe_{2-x}O_4$ ferrites with different Sm (x) content

Composition	Permeability (μ)	Saturation magnetization (emu/cm^3)	Resistivity (Ω/cm)
$x = 0.00$	150	222.22	3.3×10^6
$x = 0.025$	236	332.95	2.7×10^7
$x = 0.05$	312	360.35	5.4×10^7
$x = 0.075$	200	310.90	2.1×10^7

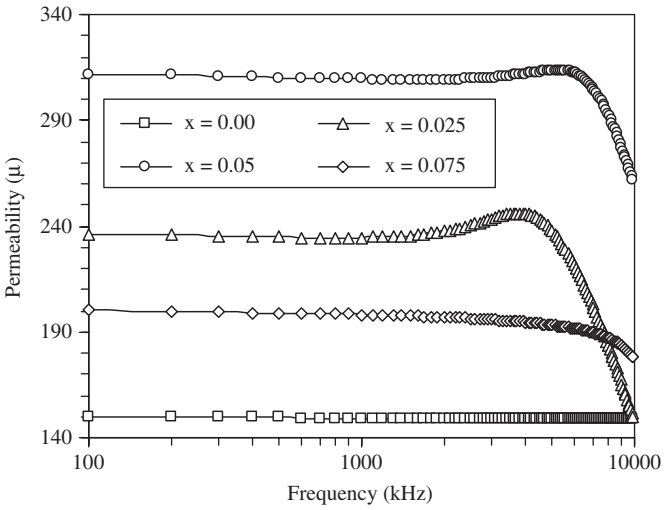

Fig. 4. Frequency dependency of permeability in different $Ni_{0.25}Cu_{0.2}Zn_{0.55}Sm_xFe_{2-x}O_4$ ferrites.

inversely proportional with magnetic permeability [19]. Also the fact is; permeability (μ_0) and resonance frequency (ω_x) are not independent, but are related by $\mu_0^2\omega_x = \text{constant}$ [20].

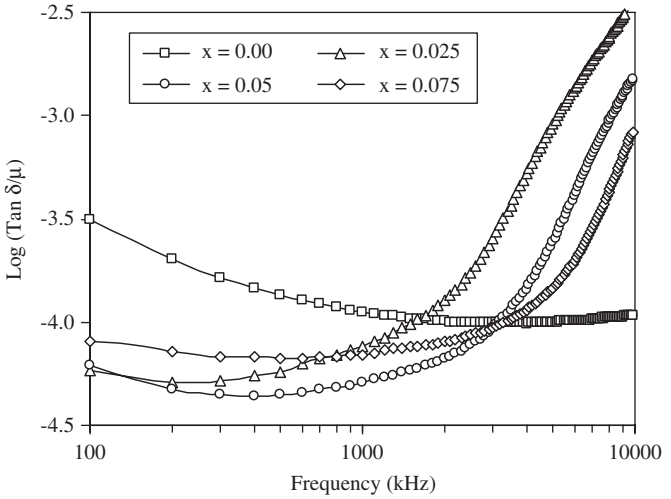

Fig. 5. Relative loss factor as a function of frequency in different $Ni_{0.25}Cu_{0.2}Zn_{0.55}Sm_xFe_{2-x}O_4$ ferrites.

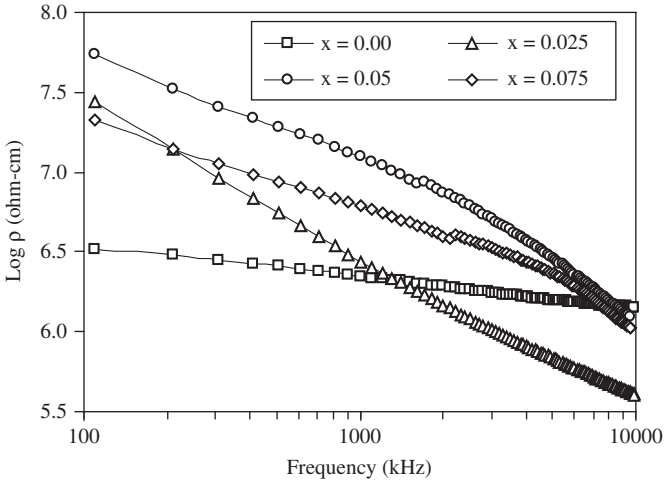

Fig. 7. AC resistivity as a function of frequency in different $Ni_{0.25}Cu_{0.2}Zn_{0.55}Sm_xFe_{2-x}O_4$ ferrites.

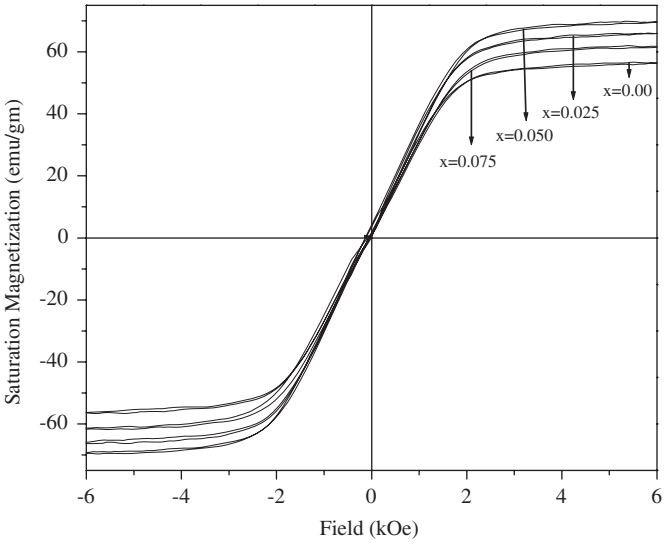

Fig. 6. Magnetic hysteresis loop for different $Ni_{0.25}Cu_{0.2}Zn_{0.55}Sm_xFe_{2-x}O_4$ ferrites.

Fig. 5 shows the relative loss factor (RLF), i.e., the ratio of the magnetic loss tangent to initial permeability. RLF (up to a frequency about 2 MHz) of the ferrite decreased with Sm substitution. The higher RLF of un-substituted ferrite may be due to higher hysteresis loss of the specimen, which may arise from its porous (porosity ~30%) structure. In general, hysteresis loss increases with increasing porosity [21]. RLF of all specimens increased after about 2 MHz frequencies due to resonance-relaxation losses. The composition with $x = 0.05$, has lowest RLF and hence will be the best material for applications up to about 2 MHz frequency.

Fig. 6 shows the magnetic loop of different $Ni_{0.25}Cu_{0.2}Zn_{0.55}Sm_xFe_{2-x}O_4$ ferrites. Saturation magnetization (M_s) values of different compositions are given in Table 2. The M_s of substituted ferrites was higher than un-substituted specimen, may be due to higher permeability of substituted ferrites. The M_s of $x = 0.075$ specimen was lower than $x = 0.05$ specimen due to its ($x = 0.075$) lower permeability as stated above.

Fig. 7 shows the frequency dependency of AC resistivity for different specimen. The resistivity (ρ) was calculated using the formula: $\rho = 1/(\omega\varepsilon_0 k' \tan\delta)$, where ε_0 is the permittivity of free space, k' is the relative dielectric constant, $\tan\delta$ is dissipation factor and ω is the angular frequency. The resistivity was increased with Sm substitution. The conduction in ferrite is considered to occur by the electron hopping between Fe^{2+} and Fe^{3+} ions those locating at octahedral site of the spinel ferrite structure. The specimen with $x = 0.05$ showed highest resistivity among all, which may be attributed to the presence of lower amount of Fe^{2+} ions in the ceramics. As described earlier, Sm-substituted compositions are deficient in Fe content and the crystallization of $SmFeO_3$ at their grain boundaries impedes the oxidation of Fe^{+3} ions inside the grains. Hence, Fe^{+2} ions are expected to be at minimum in Sm-substituted ceramics. This may be a reason of increased resistivity in them.

4. Conclusion

The substitution of Sm for Fe in $Ni_{0.25}Cu_{0.2}Zn_{0.55}Sm_xFe_{2-x}O_4$ ferrite revealed mainly the formation of secondary phase $SmFeO_3$. Relative density and grain size of the ferrite increased with increasing Sm substitution. Increased densification may be due to the appearance of excess Ni, Cu and Zn compared with Fe in the composition. A significant increase in initial permeability of the ferrite was found at small fraction ($x = 0.05$) of Sm substitution. The increased permeability was due to better densification and increased grain size in substituted ceramics. The AC resistivities of substituted ferrites were also increased due to the lowering of Fe^{+2} ion concentration. The composition $Ni_{0.25}Cu_{0.2}Zn_{0.55}Sm_{0.05}Fe_{1.95}O_4$ showed the best electromagnetic properties among all specimens and would be a better material for MLCI applications.

Acknowledgments

Author, J. Bera wishes to thank the Department of Science & Technology, Government of India, New Delhi, for providing financial support through project grant (Grant no. SR/S3/ME/04/2002-SERC-Engg).

References

[1] T. Nakamura, J. Magn. Magn. Mater. 168 (1997) 285.
[2] T.T. Ahmed, I.Z. Rahman, M.A. Rahman, J. Mater. Process. Technol. 153 (2004) 797.

[3] R. Lebourgeois, S. Duguey, J.P. Ganne, J.M. Heintz, J. Magn. Magn. Mater. 312 (2007) 328.
[4] Hua Su, H. Zhang, X. Tang, X. Xiang, J. Magn. Magn. Mater. 283 (2004) 157.
[5] Bo Li, Z.-X. Yue, Xi-Wei Qi, Ji Zhou, Zhi-Lun Gui, Long-Tu Li, Mater. Sci. Eng. B 99 (2003) 252.
[6] Kwang-Soo Park, Joong-Hee Nam, Jae-Hee Oh, J. Magn. Magn. Mater. 1415 (2001) 226.
[7] H. Su, H. Zhang, X. Tang, Y. Shi, J. Magn. Magn. Mater. 320 (2008) 483.
[8] S.R. Murthy, J. Mater. Sci. Lett. 21 (2002) 657.
[9] M. Fujimoto, J. Am. Ceram. Soc. 77 (1994) 2873.
[10] E. Rezlescu, N. Rezlescu, P.D. Popa, L. Reslescu, C. Pasnicu, Phys. Status Solidi A 162 (1997) 673.
[11] L. Zhao, H. Yang, L. Yu, Y. Cui, X. Zhao, S. Feng, J. Magn. Magn. Mater. 305 (2006) 91.
[12] A.A. Sattar, A.H. Wafik, K.M. El-Shokrofy, M.M. El-Tabby, Phys. Status Solidi A 171 (1999) 563.
[13] S.E. Jacobo, S. Duhalde, H.R. Bertorello, J. Magn. Magn. Mater. 272–276 (2004) 2253.
[14] P.K. Roy, J. Bera, J. Magn. Magn. Mater. 320 (2008) 1128.
[15] P.K. Roy, J. Bera, Mater. Res. Bull. 42 (2007) 77.
[16] K.O. Low, F.R. Sale, J. Magn. Magn. Mater. 246 (2002) 30.
[17] A.C.F.M. Costa, M.R. Morelli., R.H.G.A. Kiminami, J. Mater. Sci. 39 (2004) 1773.
[18] J.J. Shrotri, S.D. Kulkarni, C.E. Deshpande, S.K. Dtate, Mater. Chem. Phys. 59 (1999) 1.
[19] Y. Bai, J. Shou, Z. GUi, Z. YUe, L. Li, J. Magn. Magn. Mater. 264 (2003) 44.
[20] R. Valenzuela, Magnetic Ceramics, National University of Mexico, 1994.
[21] L. Neel, Physica 15 (1949) 225.